

Spectrally Distilled Representations Aligned with Instruction-Augmented LLMs for Satellite Imagery

Minh Kha Do¹ Wei Xiang^{1*} Kang Han¹ Di Wu¹ Khoa Phan¹
 Yi-Ping Phoebe Chen¹ Gaowen Liu² Ramana Rao Kompella²

¹La Trobe University, Melbourne, VIC 3086, Australia ²Cisco Research, San Jose, CA, USA

{m.do, w.xiang, k.han, d.wu, k.phan, phoebe.chen}@latrobe.edu.au,
 {gaoliu, rkompell}@cisco.com

Abstract

Vision-language foundation models (VLFMs) promise zero-shot and retrieval understanding for Earth observation. While operational satellite systems often lack full multi-spectral coverage, making RGB-only inference highly desirable for scalable deployment, the adoption of VLFMs for satellite imagery remains hindered by two factors: (1) multi-spectral inputs are informative but difficult to exploit consistently due to band redundancy and misalignment; and (2) CLIP-style text encoders limit semantic expressiveness and weaken fine-grained alignment. We present SATtxt, a spectrum-aware VLFM that operates with RGB inputs only at inference while retaining spectral cues learned during training. Our framework comprises two stages. First, Spectral Representation Distillation transfers spectral priors from a frozen multi-spectral teacher to an RGB student via a lightweight projector. Second, Spectrally Grounded Alignment with Instruction-Augmented LLMs bridges the distilled visual space and an expressive LLM embedding space. Across EuroSAT, BigEarthNet, and ForestNet, SATtxt improves zero-shot classification on average by 4.2%, retrieval by 5.9%, and linear probing by 2.7% over baselines, showing an efficient path toward spectrum-aware vision-language learning for Earth observation. Project page: <https://ikhado.github.io/sattxt/>

1. Introduction

Vision-language foundation models (VLFMs) align visual and textual concepts through large-scale contrastive training and have reshaped representation learning [1, 49]. Pioneering examples include SigLIP [40] and DINOtxt [17], which demonstrate that language supervision can drive broad generalization across modalities. This capability is especially valuable for satellite imagery, where exhaustive labels are

*Corresponding author.

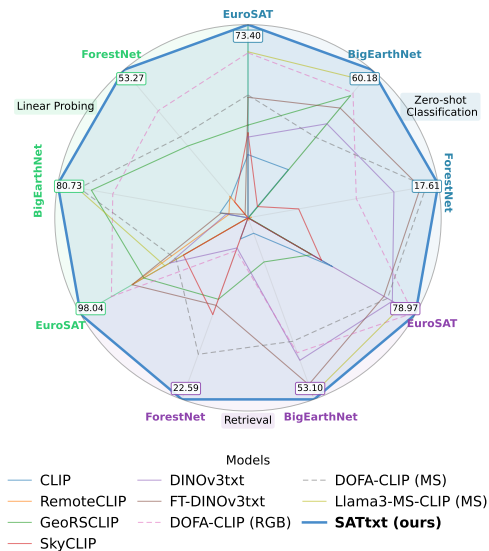


Figure 1. SATtxt outperforms existing VLFMs across three satellite benchmarks while requiring only RGB inputs. By contrast, multi-spectral VLFMs (e.g., DOFA-CLIP [46]) exhibit inconsistent gains from multi-spectral (MS) inputs.

rare and annotation often requires domain experts [14, 26]. In this context, VLFMs make zero-shot use practical by enabling classification and retrieval, such as identifying land-cover types or rare phenomena directly from prompts [20]. However, current VLFMs face key limitations when applied to satellite imagery, motivating the need for spectrum-aware and semantically expressive models.

Meanwhile, satellites continuously collect vast amounts of unlabeled imagery from missions such as Sentinel and Landsat [38, 41, 45]. However, progress in VLFMs remains constrained by the scarcity of high-quality image-text pairs [37, 47], creating a mismatch between abundant visual data and limited aligned descriptions that impedes scalable training of standard VLFMs. While recent efforts Llama3-

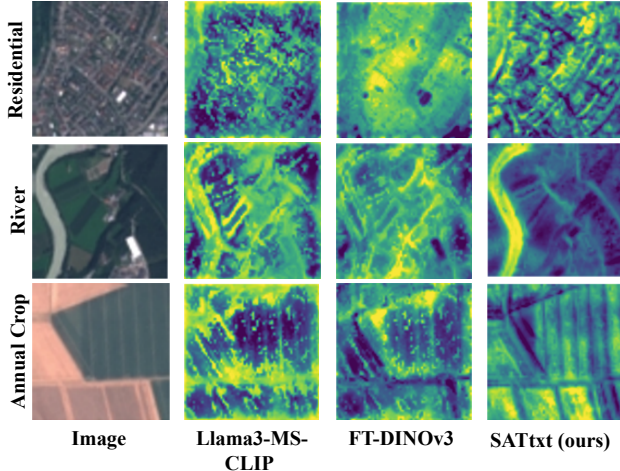


Figure 2. Patch-wise similarity between images and label prompts for models pre-trained on the same dataset. FT-DINOv3txt denotes DINOv3txt further pre-trained on this dataset, consistent with Llama3-MS-CLIP and SATtxt. Using an instruction-augmented LLM as the text encoder, our method produces sharper object-level focus (*e.g.*, river) and clearer contextual relations (*e.g.*, residential), supporting strong zero-shot predictions.

MS-CLIP [27], and DOFA-CLIP [46] report encouraging zero-shot results, two key challenges still hinder their effective deployment for satellite imagery.

First, satellite imagery commonly comprises multi-spectral inputs, yet existing models often fail to exploit them effectively. While additional bands provide complementary information, they also introduce redundancy and inter-band misalignment [27, 34]. Empirical studies [27] show that adding spectral bands yields diminishing or unstable gains. For instance, Fig. 1 illustrates DOFA-CLIP [46] achieving fluctuating gains. In addition, Llama3-MS-CLIP [27] observes degradation beyond ten bands. Moreover, complete spectral stacks are not always available due to atmospheric conditions or sensor degradation [29]. These factors motivate the development of an RGB-only VLFM that exploits prior spectral knowledge while avoiding the redundancy and misalignment of explicit multi-spectral stacks. We show that such a model can often match or exceed the performance of MS models on standard benchmarks.

Second, recent VLFMs for satellite imagery remain constrained by the limited representational capacity of the CLIP-style text encoder. Prior approaches such as RemoteCLIP [22], GeoRSCLIP [50], and Llama3-MS-CLIP [27] continue to pre-train or extend both CLIP encoders. Other approaches, such as DOFA-CLIP [46], which freezes the text encoder, and DINOv3txt, which adopts a LiT-like design [48] that freezes the vision backbone, still depend on a comparatively lightweight text encoder. Across these variants, the text encoder remains the persistent bottleneck, re-

stricting textual expressivity and weakening fine-grained cross-modal alignment. In contrast, advances in large language models (LLMs) demonstrate that instruction-augmented language representations can produce more expressive embeddings [4, 24, 36]. Building on this insight, we employ an instruction-augmented LLM to generate dense text embeddings that replace standard CLIP text features. As illustrated in Fig. 2, these LLM-derived embeddings enhance object-level focus and contextual reasoning, leading to consistent gains in downstream tasks.

To address the aforementioned challenges, we propose SATtxt, an RGB-only VLFM for satellite imagery that retains spectral cues and rich language grounding. Our model is pre-trained in two stages. First, **Spectral Representation Distillation** (SRD) transfers knowledge from a multi-spectral encoder to an RGB encoder via a lightweight projector. The projector reconstructs multi-spectral representations from RGB representations, enabling the model to effectively exploit spectral knowledge. Second, **Spectrally Grounded Alignment with Instruction-Augmented LLMs** (SGI-LLM) aligns the spectrally distilled representations with instruction-augmented LLMs via lightweight projectors trained under a contrastive learning objective. By exploiting the richer semantics of instruction-augmented LLMs, this stage overcomes the limitations of CLIP-style text encoders and yields stronger cross-modal representations. This frozen-backbone design substantially reduces pre-training cost.

In summary, our contributions are threefold. (1) We propose SATtxt, a spectrum-aware VLFM for satellite imagery that leverages spectral priors while operating exclusively on RGB inputs at inference. (2) We propose Spectral Representation Distillation (SRD), which transfers multi-spectral priors into an RGB-based representation space, enabling spectrum-aware reasoning without multi-spectral inputs during inference. (3) We design Spectrally Grounded Alignment with Instruction-Augmented LLMs (SGI-LLM), an alignment stage that bridges spectrally distilled visual representations into the space of instruction-augmented LLM embeddings via lightweight projectors, thereby producing spectrally grounded and semantically expressive cross-modal representations. Extensive experiments across four benchmarks, *i.e.*, EuroSAT, BigEarthNet, ForestNet, and DFC2020 demonstrate that SATtxt outperforms multi-spectral baselines in zero-shot classification, text-image retrieval, open vocabulary segmentation and linear probing.

2. Related Work

2.1. Representation Learning in Remote Sensing

Remote sensing (RS) foundation models aim to support diverse downstream tasks with limited annotation and min-

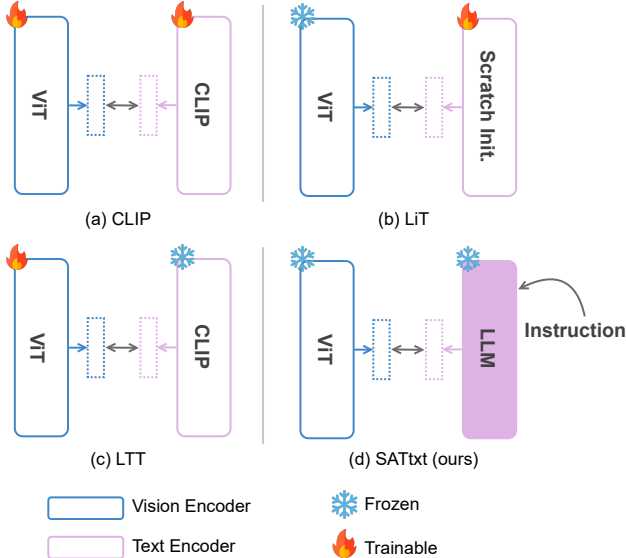


Figure 3. Pre-training strategies for VLFMs on satellite imagery. (a) CLIP-style continued pre-training (e.g., RemoteCLIP), (b) LiT: Locked-image Tuning (e.g., DINOv3txt), (c) LTT: Locked-text Tuning (e.g., DOFA-CLIP), and (d) SATtxt: bridges two strong, frozen encoders via instruction-augmented text from an LLM, improving training efficiency as well as zero-shot and linear-probe performance.

imal adaptation [21, 26]. Most existing RS pre-training pipelines follow self-supervised learning (SSL), particularly masked image modeling (MIM) [8, 11, 39] variants such as SatMAE [7, 30], Scale-MAE [33], and Spectral-GPT [13], or multi-modal extensions such as CROMA [9], Skysense [10], and Terramind [16]. While reconstruction objectives effectively learn spatial and spectral priors, they tend to emphasize low-level statistics, often requiring heavy task-specific tuning to obtain high-level semantic capability [2]. Beyond MIM, self-distillation approaches [3, 6] match representations across augmented views, obviating the need for explicit part reconstruction within the JEPA framework [2] and obtaining strong performance. However, they typically require teacher and student to share architecture and modality, provide no mechanism to inject language semantics or spectral cues. This limits their ability to generalize to heterogeneous inputs and open-vocabulary settings.

We introduce SRD, a cross-modal knowledge distillation framework that transfers spectral priors from MS imagery to RGB models. While various forms of knowledge distillation exist for remote sensing [10, 23, 43], the key idea in SRD is a cross-modal, unidirectional distillation from an MS teacher to an RGB student through a lightweight projector. This mechanism is specifically designed to imbue an RGB encoder with spectral knowledge without requiring MS inputs at inference. Unlike existing methods [6, 31], the two operate on different modalities and may use distinct,

modality-specific backbones. Moreover, both encoders stay frozen. Consequently, a lightweight projector is the only trainable module, aligning RGB features to the teacher’s MS space and thus transferring spectral knowledge for efficient adaptation without full fine-tuning.

2.2. Vision-Language Foundation Models for Remote Sensing

Contrastive learning VLFMs demonstrate strong zero-shot transfer by aligning images and text in a shared embedding space [19, 40]. In remote sensing, representative adaptations include RemoteCLIP [22], SkyCLIP [42], and GeoRSCLIP [50], which are trained on large-scale RS RGB datasets whose textual descriptions are primarily derived from labeled categories or short annotations. While effective, such captions are brief and semantically shallow, which can limit generalization. More recently, Llama3-MS-CLIP [27] extends alignment to multi-spectral (MS) imagery by pairing MS images with rich and detailed descriptions, and DOFA-CLIP [46] introduces modality-aware knowledge aggregation together with wavelength-based patch embeddings [44] to accommodate varying spectral bands. Despite these advances, current RS VLFMs still face challenges in fully exploiting multi-spectral inputs, and their representation richness can be constrained by conventional text encoders.

Fig. 3 illustrates that prior work typically employs either a CLIP text encoder or a text encoder trained from scratch (scratch init.) and fine-tunes at least one encoder. By contrast, SATtxt follows a different learning pattern. Specifically, we freeze both the RGB vision encoder and the LLM-based text encoder, and train only lightweight projectors. Spectral knowledge is distilled via cross-modal distillation from the MS teacher into the frozen RGB encoder, and cross-modal alignment is achieved by connecting this spectrally informed RGB space to a frozen instruction-augmented LLM. This design yields RGB-only inference and stronger zero-shot transfer with a low pre-training cost.

3. Method

In this section, we detail SATtxt. Fig. 4 illustrates the two pre-training stages.

3.1. Spectral Representation Distillation

Multi-spectral imagery includes both visible (RGB) and non-visible bands, providing richer spectral cues than RGB alone. However, directly relying on MS inputs yields inconsistent performance gains [27] and reduces deployability at test time. To bridge this gap, we train a lightweight projector to reconstruct MS representations from RGB features, transferring spectral priors to the RGB encoder. This enables spectrum-aware representations while requiring only

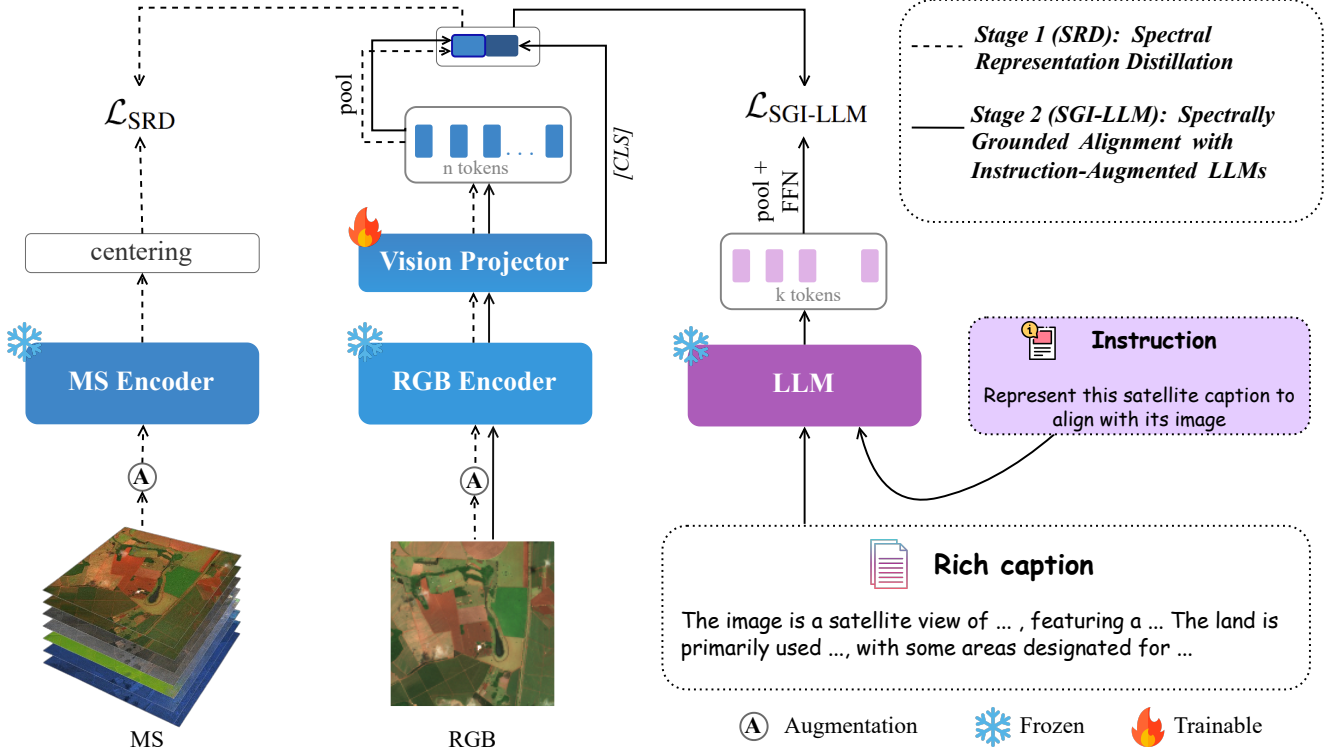


Figure 4. Two-stage pre-training pipeline for SATxt. **Stage 1 (SRD)** - dashed lines: a vision projector is trained to reconstruct multi-spectral representations from an RGB encoder by distilling a frozen MS teacher, transferring spectral knowledge so MS inputs are unnecessary in Stage 2 and at inference. **Stage 2 (SGI-LLM)** - solid lines: with vision and text encoders frozen, distilled vision features are aligned with LLM-based text embeddings using instruction-augmented prompts, enhancing cross-modal representations while preserving pretrained capabilities.

RGB inputs during inference. The overall training procedure is summarized in Algorithm 1.

Given an MS image \mathbf{x}_{ms} , we construct two augmented view sets: an MS set \mathcal{V}_{ms} and an RGB set \mathcal{V}_{rgb} . The MS set contains full-resolution, full-band *global* views and is encoded by a frozen, pretrained MS encoder \mathcal{E}_{ms} to produce teacher pre-softmax outputs. The RGB set follows a multi-crop strategy with local crops $\mathcal{V}_{\text{rgb}}^{\text{local}}$ and full-resolution global views $\mathcal{V}_{\text{rgb}}^{\text{global}}$, such that $\mathcal{V}_{\text{rgb}} = \mathcal{V}_{\text{rgb}}^{\text{local}} \cup \mathcal{V}_{\text{rgb}}^{\text{global}}$. These RGB views are encoded by a frozen, pretrained RGB encoder \mathcal{E}_{rgb} . A lightweight projector $\mathcal{G}_v : \mathbb{R}^{d_{\text{rgb}}} \rightarrow \mathbb{R}^K$ is the only trainable module, mapping RGB representations into the MS representation space of dimension K , where K denotes the patch embedding dimensionality of the MS encoder. For each RGB view $v \in \mathcal{V}_{\text{rgb}}$ and MS view $u \in \mathcal{V}_{\text{ms}}$,

$$\mathbf{z}_v^{\text{rgb}} = \mathcal{E}_{\text{rgb}}(\tilde{\mathbf{x}}_{\text{rgb}}^{(v)}) \in \mathbb{R}^{d_{\text{rgb}}}, \quad (1)$$

$$\mathbf{z}_u^{\text{ms}} = \text{Pool}(\mathcal{E}_{\text{ms}}(\tilde{\mathbf{x}}_{\text{ms}}^{(u)})) \in \mathbb{R}^K, \quad (2)$$

$$\hat{\mathbf{z}}_v^{\text{ms}} = \mathcal{G}_v(\mathbf{z}_v^{\text{rgb}}) \in \mathbb{R}^K, \quad (3)$$

where tildes denote augmented views and $\text{Pool}(\cdot)$ is patch-wise average pooling over MS tokens. Intuitively, the pro-

jector \mathcal{G}_v learns to map RGB features into the MS teacher’s embedding space, allowing each RGB view to be represented as if it had been observed in multi-spectral bands. The resulting RGB encoder, equipped with distilled spectral priors, serves as initialization for the subsequent LLM-alignment stage.

Training adopts the centering and temperature sharpening strategy of DINO [6]. However, in DINO, the teacher network is updated via exponential moving average of the student, whereas here the teacher is a frozen, pretrained MS encoder. Let $\boldsymbol{\mu} \in \mathbb{R}^K$ denote an exponential moving average of the teacher’s pre-softmax outputs with momentum m_c , and let $\tau_t < \tau_s$ be the temperature parameters for the teacher and student, respectively. We define

$$\mathbf{q}_u = \text{softmax}\left(\frac{\mathbf{z}_u^{\text{ms}} - \boldsymbol{\mu}}{\tau_t}\right), \quad \mathbf{p}_v = \text{softmax}\left(\frac{\hat{\mathbf{z}}_v^{\text{ms}}}{\tau_s}\right), \quad (4)$$

and minimize the average cross-entropy over all RGB-MS view pairs

$$\mathcal{L}_{\text{SRD}} = \frac{1}{|\mathcal{V}_{\text{rgb}}| |\mathcal{V}_{\text{ms}}|} \sum_{v \in \mathcal{V}_{\text{rgb}}} \sum_{u \in \mathcal{V}_{\text{ms}}} [-\mathbf{q}_u^\top \log \mathbf{p}_v]. \quad (5)$$

Algorithm 1 Spectral Representation Distillation (PyTorch-like pseudocode; multi-crop omitted for clarity)

```

# e_rgb, e_ms: frozen RGB and MS encoders
# g: trainable projector mapping RGB to MS space
# C: EMA center in R^K
# T_t < T_s: temperatures; m: center momentum

for x_ms, x_rgb in loader: # paired MS/RGB minibatch
    u, v = aug_ms(x_ms), aug_rgb(x_rgb)

    t = e_ms(u) # teacher logits in R^K
    s = g(e_rgb(v)) # student logits in R^K

    q = softmax((t - C) / T_t, dim=1)
    p = softmax(s / T_s, dim=1)

    loss = -(q * log(p)).sum(dim=1).mean()
    loss.backward()
    update(g) # update projector only

with torch.no_grad(): # EMA center update
    C = m*C + (1 - m)*t.mean(dim=0)

```

This objective encourages each RGB view to match the distribution of its MS teacher, thereby transferring spectral priors into the RGB encoder.

Only the projector \mathcal{G}_v is updated during training, while both \mathcal{E}_{rgb} and \mathcal{E}_{ms} remain frozen. Let $\text{sg}(\cdot)$ denote the stop-gradient operator, defined as $\text{sg}(\mathbf{z}) = \mathbf{z}$ in the forward pass and $\partial \text{sg}(\mathbf{z})/\partial \mathbf{z} = 0$ during backpropagation. The center update is given by

$$\boldsymbol{\mu} \leftarrow m_c \boldsymbol{\mu} + (1 - m_c) \frac{1}{|\mathcal{V}_{\text{ms}}|} \sum_{u \in \mathcal{V}_{\text{ms}}} \text{sg}(\mathbf{z}_u^{\text{ms}}). \quad (6)$$

After distillation, the projector \mathcal{G}_v learns to reconstruct MS representations from RGB input alone, allowing all subsequent stages and inference to operate solely on RGB inputs.

Our method extends DINO’s centering and temperature sharpening with three adaptations for spectral-to-RGB transfer. First, the teacher is a fixed MS encoder, providing a stable spectral reference and preventing drift when RGB features must capture information beyond their spectral range. Second, both encoders are frozen and only the lightweight projector is trained, concentrating capacity on cross-modal mapping while reducing overfitting and computational cost. Third, we perform cross-modal alignment by pairing RGB views with MS teacher outputs, using multi-crop augmentations for RGB and global views for MS. This asymmetric design enhances RGB diversity while maintaining a coherent spectral target. MS inputs are used only once during SRD to distill spectral knowledge. Stage 2 and downstream tasks operate only on RGB imagery.

3.2. Spectrally Grounded Alignment with Instruction-Augmented LLMs

In contrastive learning, the expressive capacity of modal-ity encoders is crucial. Many remote-sensing VLFMs still rely on conventional text encoders, which limits semantic richness. Recent studies demonstrate that LLMs serve not

only as strong generators but also as competitive text encoders [4, 36]. Unlike LiT [48], which freezes a powerful image encoder while updating the text encoder, we employ an LLM as the text encoder, freeze both encoders, and train only lightweight projectors for alignment. This design preserves pretrained capabilities while yielding richer and more expressive cross-modal representations.

Given an RGB image \mathbf{x}_{rgb} and a composite textual prompt consisting of a caption \mathcal{C} and an instruction \mathcal{I} , the frozen image encoder and learned projector produce $\mathbf{H}_v = \mathcal{G}_v(\mathcal{E}_{\text{rgb}}(\mathbf{x}_{\text{rgb}})) \in \mathbb{R}^{(1+n) \times d_v}$, while the LLM-based text encoder generates $\mathbf{H}_t = \text{LLM}(\mathcal{C}, \mathcal{I}) \in \mathbb{R}^{k \times d_t}$. Here, \mathbf{H}_v contains one class token and n patch tokens of width d_v , and \mathbf{H}_t consists of k token-level embeddings of width d_t . Following DINOxt [17, 35], we concatenate the class token with the mean of patch tokens to form a compact and robust visual descriptor \mathbf{z}_v as

$$\mathbf{z}_v = [\mathbf{H}_v^{(\text{cls})}; \text{mean}(\mathbf{H}_v^{\text{patch}})] \in \mathbb{R}^{2d_v}. \quad (7)$$

The frozen LLM encodes the instruction-augmented prompt $(\mathcal{C}, \mathcal{I})$. Mean pooling over all token embeddings produces a sentence-level representation $\tilde{\mathbf{z}}_t$, which is subsequently projected into the shared vision-language space

$$\tilde{\mathbf{z}}_t = \text{mean}(\mathbf{H}_t) \in \mathbb{R}^{d_t}, \quad \mathbf{z}_t = \mathcal{G}_t(\tilde{\mathbf{z}}_t) \in \mathbb{R}^{2d_v}, \quad (8)$$

where \mathcal{G}_t is a lightweight linear projector. This projection aligns the LLM-derived textual embedding with the visual descriptor \mathbf{z}_v in a unified feature space.

Using LLM as the text encoder offers two key advantages. First, since LLM is frozen, \mathbf{H}_t can be precomputed and cached once per prompt, significantly reducing training time. Second, unlike traditional text encoders with limited token budgets (*e.g.*, 77 tokens in CLIP [32]), the LLM encoder supports longer instruction-augmented inputs $(\mathcal{C}, \mathcal{I})$, providing richer semantics and task-aware signals that strengthen cross-modal alignment.

Contrastive objective. We align the visual and textual embeddings \mathbf{z}_v and \mathbf{z}_t using a symmetric InfoNCE objective over a mini-batch \mathcal{B} . Let $s(\cdot, \cdot)$ denote cosine similarity and τ the temperature parameter. The image-to-text and text-to-image contrastive losses are defined as

$$\begin{aligned} \mathcal{L}_{v \rightarrow t} &= -\frac{1}{|\mathcal{B}|} \sum_{i \in \mathcal{B}} \log \frac{\exp(s(\mathbf{z}_{v,i}, \mathbf{z}_{t,i})/\tau)}{\sum_{j \in \mathcal{B}} \exp(s(\mathbf{z}_{v,i}, \mathbf{z}_{t,j})/\tau)}, \\ \mathcal{L}_{t \rightarrow v} &= -\frac{1}{|\mathcal{B}|} \sum_{i \in \mathcal{B}} \log \frac{\exp(s(\mathbf{z}_{t,i}, \mathbf{z}_{v,i})/\tau)}{\sum_{j \in \mathcal{B}} \exp(s(\mathbf{z}_{t,i}, \mathbf{z}_{v,j})/\tau)}. \end{aligned} \quad (9)$$

The final training objective averages both directions

$$\mathcal{L}_{\text{SGI-LLM}} = \frac{1}{2} (\mathcal{L}_{v \rightarrow t} + \mathcal{L}_{t \rightarrow v}). \quad (10)$$

This symmetric formulation ensures bidirectional consistency between the visual and textual modalities.

At inference time, textual embeddings for the label set can be precomputed and cached once, so that the per-query cost is dominated by a single forward pass through the RGB vision encoder and the projectors. Consequently, employing a large LLM-based text encoder does not significantly impact online latency.

4. Experiments

Pre-training. We use SSL4EOS12 [5], a widely used dataset for geospatial foundation models [16, 27], as the training set for both stages. The dataset comprises approximately 1 M images with 12 spectral bands and global geographic coverage. The image-caption pairs are from the public Llama3-SSL4EO-S12 v1.1 caption set [27], the same dataset used by Llama3-MS-CLIP. The RGB encoder is the distilled ViT-L variant of DINOv3 [35] pretrained on satellite imagery. In the first stage, the MS teacher is Spectral-GPT [13], a pre-trained MIM model for MS data. The vision projector remains lightweight, mirroring the DINOtxt configuration with two transformer blocks. In the second stage, the text encoder is Llama-3.1-8B initialized from LLM2Vec [4]. We hold both encoders fixed, pre-compute and cache the text embeddings. All stages are conducted on $8 \times$ NVIDIA H200 GPUs (141 GB each). Stage 1 runs for ~ 4 hours and Stage 2 for ~ 3 hours, for a total of ~ 7 hours of pre-training.

Downstream datasets. We evaluate on three unseen satellite benchmarks: EuroSAT [12], BigEarthNet [38], and ForestNet [15]. EuroSAT and BigEarthNet are derived from Sentinel-2 imagery. The dataset details can be found in the Supplementary Material.

Baselines. We evaluate the proposed method against VLFMs in both general-purpose and remote sensing domains. The models and their vision-input types are summarized in Tab. 1. While most baselines accept only RGB inputs, Llama3-MS-CLIP [27] and DOFA-CLIP [46] are early models that support MS inputs. The released Llama3-MS-CLIP weights handle only 10 spectral bands, whereas DOFA-CLIP [46] accommodates variable band configurations. Consequently, it is not applicable to the ForestNet dataset (5 bands), and we mark the corresponding table entries with “-”. For fairness, we also fine-tune DINOv3txt on the same training data as our method, denoted FT-DINOv3txt. Consequently, the SATtxt, Llama3-MS-CLIP, and FT-DINOv3txt models are all trained on the same SSL4EO-S12 dataset.

Downstream tasks. We evaluate models on four fundamental downstream tasks, *i.e.*, zero-shot classification, text-to-image retrieval, open-vocabulary segmentation, and linear probing. For zero-shot classification and text-to-image retrieval, we follow the evaluation protocol of Clive *et al.* [27]. For zero-shot classification, we adopt the prompt template from GeoRSClip [50] for each class. For

BigEarthNet, we adopt the setup of Clive *et al.* [27], treating the task as multi-label and decomposing it into K one-vs-rest binary classifiers. We therefore report accuracy following the Llama3-MS-CLIP setup for fair comparison, while F1 scores are provided in the Supplementary Material. For text-to-image retrieval, we compute the similarity between a given text label and all test images, rank the scores in descending order, and compute the mean average precision over the top 100 results. We report the class-averaged mAP@100. In addition, for the open vocabulary, we follow the decoder-free approach from DINOtxt [17]. For this task, we use DFC2020 dataset with Sentinel-2 images.

For linear probing, we follow the PANGAEA setup [28]. We extract final-layer representations from the models and train a single linear classifier on top. On BigEarthNet, due to the scale of the dataset, we additionally evaluate using only 10% of the training set following [7, 25]. We report mAP \uparrow on BigEarthNet and accuracy on the other datasets. Additionally, F1 scores and detailed implementations are provided in the Supplementary Material.

4.1. Results

Zero-shot classification & retrieval. We evaluate against both contrastive and generative multi-modal baselines, including GeoChat [18] and EarthDial [37] for classification.

Tab. 1 reports results on EuroSAT, BigEarthNet, and ForestNet. Overall, generative baselines show limited transfer to remote-sensing categories, whereas contrastive approaches yield stronger cross-modal alignment. Domain-adapted variants of CLIP improve over general-purpose CLIP, underscoring the benefit of remote sensing aware pre-training. Our SATtxt attains the strongest zero-shot performance across datasets. It consistently outperforms the best prior contrastive baselines. Notably, SATtxt retains these gains even when tested with RGB inputs, suggesting that its spectral-aware training yields a representation that transfers beyond the training sensor configuration.

Qualitative similarity maps (Fig. 5) align with the quantitative trends. SATtxt yields sharper, well-localized responses that trace linear structures (*e.g.* rivers) and separate visually similar land-cover types (*e.g.* permanent crops vs. herbaceous vegetation). Prior models show diffuse or off-target activations. Fig. 6 presents UMAP embeddings for the second-best model, Llama3-MS-CLIP, computed with the same configuration reported in that work. Relative to Llama3-MS-CLIP, SATtxt forms more compact clusters with clearer separation. The classes “Herbaceous Vegetation” and “Forest” overlap under Llama3-MS-CLIP, whereas our model separates them. These results indicate that explicit spectral cues and stronger fine-grained text-image alignment are crucial for effective zero-shot transfer.

Open vocabulary segmentation. Consistent with the patch-wise image-text similarity maps employed in open-

Table 1. Zero-shot classification and text-to-image retrieval on three satellite benchmarks. The “Locked? 🗝️” column indicates whether the text/vision encoders are frozen or adapter-tuned (✓/LoRA) vs. fully unfrozen (✗). “-” denotes an unsupported task or an inapplicable dataset.

Training Approach	Model	Input	Locked? 🗝️		Zero-shot Classification			Retrieval		
			Text	Vision	EuroSAT	BigEarthNet	ForestNet	EuroSAT	BigEarthNet	ForestNet
Generative	GeoChat [18]	RGB	LoRA	✗	35.00	24.16	6.31	-	-	-
	EarthDial [37]	MS	LoRA	✗	63.28	52.60	8.22	-	-	-
Contrastive	CLIP [32]	RGB	✗	✗	46.90	54.85	8.30	56.92	28.57	11.78
	RemoteCLIP [22]	RGB	✗	✗	34.02	52.28	8.46	34.34	26.62	10.35
	GeoRSCLIP [50]	RGB	✗	✗	52.92	58.80	8.33	51.36	32.80	15.84
	SkyCLIP [42]	RGB	✓	✗	51.33	52.88	10.78	53.96	26.29	16.87
	DINOv3txt [35]	RGB	✗	✓	50.48	57.30	15.44	72.84	47.33	12.38
	FT-DINOv3txt	RGB	✗	✓	58.58	58.14	16.74	70.60	50.92	16.25
	DOFA-CLIP [46]	RGB	✓	✗	67.64	58.96	13.60	78.36	46.21	12.56
	DOFA-CLIP [46]	MS	✓	✗	59.04	56.58	17.02	71.54	44.52	19.55
	Llama3-MS-CLIP [27]	MS	✗	✗	67.86	59.63	-	75.26	52.42	-
SATtxt (ours)	RGB	✓	✓	73.40	60.18	17.61	78.97	53.10	22.59	

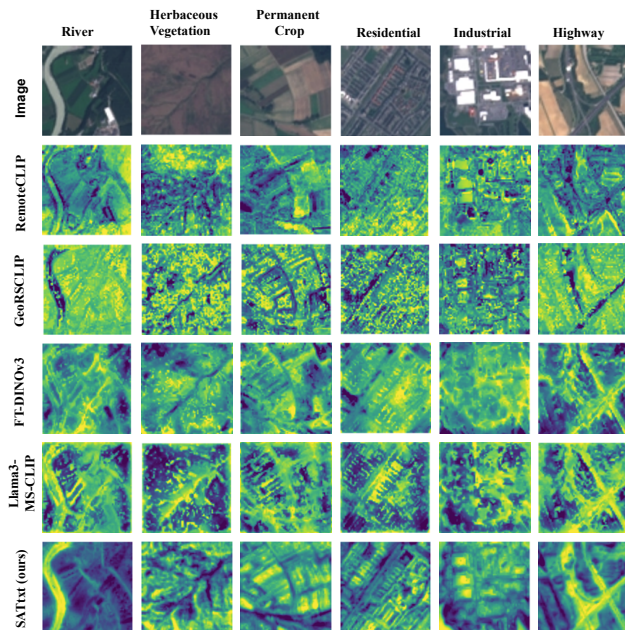


Figure 5. Patch-wise image-text similarity maps. For each image, we compute cosine similarity between patch-level vision embeddings and the text embedding produced from the prompt “a satellite image of {class}”. Compared to baselines, SATtxt yields sharper and more contiguous responses that trace class-consistent structures (e.g., linear rivers and highways) and reduce spurious activations in the background.

vocabulary segmentation, SATtxt demonstrates strong segmentation performance, achieving 31.23 mIoU. This result surpasses the state-of-the-art baseline Llama3-MS-CLIP (28.58 mIoU), which relies on multispectral inputs, as well as FT-DINOv3txt (26.81 mIoU). These comparisons indicate that SATtxt provides more accurate pixel-level align-

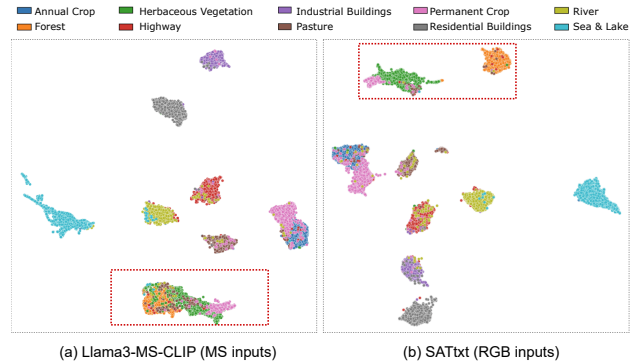


Figure 6. UMAP ($n_{\text{neighbors}} = 50$, $\text{minDist} = 0$, cosine distance) visualization of feature embeddings for (a) Llama3-MS-CLIP with MS inputs and (b) our SATtxt with RGB inputs. Points are colored by class. SATtxt yields more compact intra-class clusters and clearer inter-class separation than Llama3-MS-CLIP.

ment between visual patches and textual concepts under the open-vocabulary setting without segmentation decoder.

Linear probing. To further assess representational richness, we also compare with two recent MIM-based models, SpectralGPT and Terramind. Tab. 2 shows that domain-adapted contrastive models outperform general-purpose CLIP, with SATtxt achieving the best overall performance. While results are comparable to Terramind and other MS models when full BigEarthNet supervision is available, SATtxt yields larger gains in low-data regimes. Notably, the RGB-only SATtxt outperforms prior RGB and multispectral counterparts, indicating that the spectral-spatial pre-training objective yields embeddings that generalize under RGB-only inputs and transfer well to ForestNet.

Table 2. Linear-probe on EuroSAT, BigEarthNet (using 10% and 100% of training samples), and ForestNet. “-” denotes an inapplicable dataset.

Training Approach	Model	Input	EuroSAT		BigEarthNet		ForestNet
			10%	100%	10%	100%	
MIM	SpectralGPT [13]	MS	92.04	74.85	79.16	-	-
	Terramind [16]	MS	96.13	75.84	<u>84.68</u>	48.64	-
Contrastive	CLIP [32]	RGB	92.00	64.93	75.56	41.99	-
	RemoteCLIP [22]	RGB	96.19	64.06	75.58	42.09	-
	GeoRSCLIP [50]	RGB	95.76	77.45	81.19	46.53	-
	SkyCLIP [42]	RGB	94.33	62.20	70.12	41.58	-
	DINOv3txt [35]	RGB	94.83	64.30	70.69	40.18	-
	FT-DINOv3txt	RGB	96.18	64.81	72.83	40.48	-
	DOFA-CLIP [46]	RGB	<u>96.93</u>	75.37	81.37	<u>49.65</u>	-
	DOFA-CLIP [46]	MS	94.59	78.63	81.98	47.33	-
	Llama3-MS-CLIP [27]	MS	95.00	<u>78.90</u>	82.44	-	-
	SATtxt (ours)	RGB	98.04	80.73	84.80	53.27	-

4.2. Ablation Study

Setup. We evaluate three dimensions of ablation. First, *component ablation*: starting from a baseline (FT-DINOv3txt), we progressively add SRD (Stage 1), replace the CLIP text encoder (CLIPtext) with frozen LLM-based encoders, and finally introduce instruction-augmented prompts. Second, *text-side pooling ablation*: fixing the best component configuration, we compare pooling types for forming caption embeddings from LLM token outputs: begin-of-sequence (bos), end-of-sequence (eos), and mean pooling. Third, *MS teacher choice*: replacing the SpectralGPT with a less robust model, *i.e.*, SatMAE [7].

Component ablation results. Tab. 3 shows that SRD consistently improves the baseline, indicating that spectral distillation injects MS priors into RGB features without requiring MS inputs during later training or inference. Replacing the CLIPtext with frozen LLM encoders yields further gains, Llama-3.1-8B performs best, likely due to more expressive token-level representations and stronger context modeling. Instruction-augmented prompting adds additional improvements by embedding task-specific cues for cross-modal alignment.

Text-side pooling results. Fig. 7 illustrates mean pooling outperforms both [bos] and [eos]. This suggests that averaging token embeddings leads to a more balanced and stable sentence vector than relying on a single special token. In addition, mean pooling mitigates bias toward token saliency and is more robust to prompt-length variations. This observation aligns with LLM2Vec, which also finds mean pooling to be the most effective aggregation when adapting decoder-only LLMs for embeddings [4].

MS teacher choice results. Tab. 4 shows that SATtxt is insensitive to the choice of multi-spectral teacher: SpectralGPT and SatMAE yield closely matched performance and both surpass the strongest baselines overall. The small gap between teachers indicates that SRD reliably transfers spectral priors without hinging on a particular teacher, and

Table 3. Ablation of model components on three benchmarks. We incrementally add (i) SRD, (ii) frozen LLM text encoders, and (iii) instruction-augmented prompting. Every component yields a consistent gain, and the full model (SRD + LLM + instruction prompts) achieves the best results on all three benchmarks.

Model	EuroSAT		BigEarthNet		ForestNet	
	CLS	Retrieval	CLS	Retrieval	CLS	Retrieval
Baseline (FT-DINOv3txt)	58.6	70.6	58.1	50.9	16.7	16.3
SATtxt _{SRD} + CLIPtext	65.4	74.9	58.3	51.3	17.2	19.7
SATtxt _{SRD} + Mistral-7B	68.2	76.2	59.1	52.3	17.5	20.1
SATtxt _{SRD} + Llama-3.1-8B	70.1	76.7	59.9	52.6	17.4	22.2
SATtxt _{Llama-3.1-8B} + Inst.	65.3	74.7	58.3	50.2	16.9	22.0
SATtxt _{SRD} + Llama-3.1-8B + Inst.	73.4	79.0	60.2	53.1	17.6	22.6

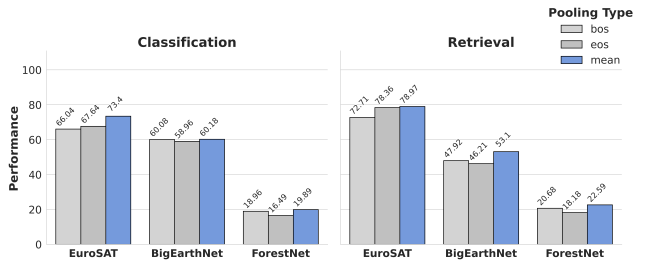


Figure 7. Ablation on text-side pooling types. Across the datasets and metrics considered, mean pooling yields the most stable and highest performance.

stronger teachers offer only modest additional gains.

Table 4. Ablation on MS teacher choice. SATtxt exhibits limited sensitivity to the choice of MS teacher.

Model	Input	EuroSAT		BigEarthNet		ForestNet	
		CLS	Retrieval	CLS	Retrieval	CLS	Retrieval
Llama3-MS-CLIP	MS	67.86	75.26	59.63	52.42	-	-
DOFA-CLIP	MS	59.04	71.54	56.58	44.52	17.02	19.55
SATtxt _{SatMAE}	RGB	<u>71.65</u>	<u>78.41</u>	59.41	53.20	<u>17.15</u>	<u>20.14</u>
SATtxt _{SpectralGPT}	RGB	73.40	78.97	60.18	<u>53.10</u>	17.61	22.59

5. Conclusion

In this paper, we proposed SATtxt, a spectrum-aware VLFM for satellite imagery that uses only RGB at inference, while transferring MS priors through Spectral Representation Distillation and aligning visual features to text embeddings from instruction-augmented LLMs. Across three satellite benchmarks, SATtxt consistently surpasses strong baselines with the largest gains on the most challenging dataset. However, the current design is restricted to optical imagery. Moreover, although label embeddings are cacheable, relying on a large LLM text encoder increases memory requirements relative to CLIP-style text encoders. Future work will extend the framework to broader sensor coverage, including SAR and thermal imagery.

6. Acknowledgement

This work was supported in part by the Australian Government through the Australian Research Council’s Discovery Projects Funding Scheme under Project DP220101634, and by the NVIDIA Academic Grant Program.

References

- [1] Mothilal Asokan, Kebin Wu, and Fatima Albreiki. FineLIP: Extending CLIP’s Reach via Fine-Grained Alignment with Longer Text Inputs . In *2025 IEEE/CVF Conference on Computer Vision and Pattern Recognition (CVPR)*, pages 14495–14504, Los Alamitos, CA, USA, 2025. IEEE Computer Society. 1
- [2] Mahmoud Assran, Quentin Duval, Ishan Misra, Piotr Bojanowski, Pascal Vincent, Michael Rabbat, Yann LeCun, and Nicolas Ballas. Self-supervised learning from images with a joint-embedding predictive architecture. In *2023 IEEE/CVF Conference on Computer Vision and Pattern Recognition (CVPR)*, pages 15619–15629, 2023. 3
- [3] Guillaume Astruc, Nicolas Gonthier, Clément Mallet, and Loic Landrieu. Anysat: One earth observation model for many resolutions, scales, and modalities. In *2025 IEEE/CVF Conference on Computer Vision and Pattern Recognition (CVPR)*, pages 19530–19540, 2025. 3
- [4] Parishad BehnamGhader, Vaibhav Adlakha, Marius Mosbach, Dzmitry Bahdanau, Nicolas Chapados, and Siva Reddy. LLM2Vec: Large language models are secretly powerful text encoders. In *First Conference on Language Modeling*, 2024. 2, 5, 6, 8
- [5] Benedikt Blumenstiel, Nassim Ait Ali Braham, Conrad M Albrecht, Stefano Maurogiovanni, and Paolo Fraccaro. SSL4EOS12 v1.1 – A Multimodal, Multiseasonal Dataset for Pretraining. *arXiv preprint arXiv:2503.00168*, 2025. 6
- [6] Mathilde Caron, Hugo Touvron, Ishan Misra, Hervé Jegou, Julien Mairal, Piotr Bojanowski, and Armand Joulin. Emerging properties in self-supervised vision transformers. In *2021 IEEE/CVF International Conference on Computer Vision (ICCV)*, pages 9630–9640, 2021. 3, 4
- [7] Yezhen Cong, Samar Khanna, Chenlin Meng, Patrick Liu, Erik Rozi, Yutong He, Marshall Burke, David B. Lobell, and Stefano Ermon. SatMAE: Pre-training transformers for temporal and multi-spectral satellite imagery. In *Advances in Neural Information Processing Systems*, 2022. 3, 6, 8, 2
- [8] Minh Kha Do, Kang Han, Phu Lai, Khoa T. Phan, and Wei Xiang. Robsense: A robust multi-modal foundation model for remote sensing with static, temporal, and incomplete data adaptability. In *Proceedings of the IEEE/CVF Conference on Computer Vision and Pattern Recognition (CVPR)*, pages 7427–7436, 2025. 3
- [9] Anthony Fuller, Koreen Millard, and James R. Green. Croma: remote sensing representations with contrastive radar-optical masked autoencoders. In *Proceedings of the 37th International Conference on Neural Information Processing Systems*, Red Hook, NY, USA, 2023. Curran Associates Inc. 3
- [10] Xin Guo, Jiangwei Lao, Bo Dang, Yingying Zhang, Lei Yu, Lixiang Ru, Liheng Zhong, Ziyuan Huang, Kang Wu, Dingxiang Hu, Huimei He, Jian Wang, Jingdong Chen, Ming Yang, Yongjun Zhang, and Yansheng Li. Skysense: A multi-modal remote sensing foundation model towards universal interpretation for earth observation imagery. In *Proceedings of the IEEE/CVF Conference on Computer Vision and Pattern Recognition (CVPR)*, pages 27672–27683, 2024. 3
- [11] Kaiming He, Xinlei Chen, Saining Xie, Yanghao Li, Piotr Dollár, and Ross Girshick. Masked autoencoders are scalable vision learners. In *2022 IEEE/CVF Conference on Computer Vision and Pattern Recognition (CVPR)*, pages 15979–15988, 2022. 3
- [12] Patrick Helber, Benjamin Bischke, Andreas Dengel, and Damian Borth. Eurosat: A novel dataset and deep learning benchmark for land use and land cover classification. *IEEE Journal of Selected Topics in Applied Earth Observations and Remote Sensing*, 12(7):2217–2226, 2019. 6
- [13] Danfeng Hong, Bing Zhang, Xuyang Li, Yuxuan Li, Chenyu Li, Jing Yao, Naoto Yokoya, Hao Li, Pedram Ghamisi, Xiuping Jia, Antonio Plaza, Paolo Gamba, Jon Atli Benediktsson, and Jocelyn Chanussot. Spectralgpt: Spectral remote sensing foundation model. *IEEE Transactions on Pattern Analysis and Machine Intelligence*, 46(8):5227–5244, 2024. 3, 6, 8
- [14] Benyamin Hosseiny, Masoud Mahdianpari, Mohammadali Hemati, Ali Radman, Fariba Mohammadimanesh, and Jocelyn Chanussot. Beyond supervised learning in remote sensing: A systematic review of deep learning approaches. *IEEE Journal of Selected Topics in Applied Earth Observations and Remote Sensing*, 17:1035–1052, 2024. 1
- [15] Jeremy Irvin, Hao Sheng, Neel Ramachandran, Sonja Johnson-Yu, Sharon Zhou, Kyle Story, Rose Rustowicz, Cooper Elsworth, Kemen Austin, and Andrew Ng. Forestnet: Classifying drivers of deforestation in indonesia using deep learning on satellite imagery, 2020. 6, 2
- [16] Johannes Jakubik, Felix Yang, Benedikt Blumenstiel, Erik Scheurer, Rocco Sedona, Stefano Maurogiovanni, Jente Bosmans, Nikolaos Dionelis, Valerio Marsocci, Niklas Kopp, et al. Terramind: Large-scale generative multimodality for earth observation. *IEEE/CVF International Conference on Computer Vision (ICCV)*, 2025. 3, 6, 8
- [17] Cijo Jose, Theo Moutakanni, Dahyun Kang, Federico Baldassarre, Timothee Darcet, Hu Xu, Daniel Li, Marc Szafraniec, Michael Ramamonjisoa, Maxime Oquab, Oriane Simeoni, Huy V. Vo, Patrick Labatut, and Piotr Bojanowski. DINOv2 Meets Text: A Unified Framework for Image- and Pixel-Level Vision-Language Alignment . In *2025 IEEE/CVF Conference on Computer Vision and Pattern Recognition (CVPR)*, pages 24905–24916, 2025. 1, 5, 6
- [18] Kartik Kuckreja, Muhammad Sohail Danish, Muzammal Naseer, Abhijit Das, Salman Khan, and Fahad Shahbaz Khan. Geochat:grounded large vision-language model for remote sensing. In *2024 IEEE/CVF Conference on Computer Vision and Pattern Recognition (CVPR)*, pages 27831–27840, 2024. 6, 7

- [19] Mengcheng Lan, Chaofeng Chen, Yiping Ke, Xinjiang Wang, Litong Feng, and Wayne Zhang. Clearclip: Decomposing clip representations for dense vision-language inference. In *Computer Vision – ECCV 2024*, pages 143–160, Cham, 2025. Springer. 3
- [20] Xiang Li, Congcong Wen, Yuan Hu, and Nan Zhou. Rs-clip: Zero shot remote sensing scene classification via contrastive vision-language supervision. *International Journal of Applied Earth Observation and Geoinformation*, 124:103497, 2023. 1
- [21] Zhihao Li, Biao Hou, Siteng Ma, Zitong Wu, Xianpeng Guo, Bo Ren, and Licheng Jiao. Masked angle-aware autoencoder for remote sensing images. In *European Conference on Computer Vision*, pages 260–278. Springer, 2025. 3
- [22] Fan Liu, Delong Chen, Zhangqingyun Guan, Xiaocong Zhou, Jiale Zhu, Qiaolin Ye, Liyong Fu, and Jun Zhou. Remoteclip: A vision language foundation model for remote sensing. *IEEE Transactions on Geoscience and Remote Sensing*, 62:1–16, 2024. 2, 3, 7, 8
- [23] Hao Liu, Ying Qu, and Liqiang Zhang. Multispectral scene classification via cross-modal knowledge distillation. *IEEE Transactions on Geoscience and Remote Sensing*, 60:1–12, 2022. 3
- [24] William D. Lukito, Wei Xiang, Chang Liu, Phu Lai, Peng Cheng, Weijie Yuan, and Guoqiang Mao. Channel-agnostic predictive beamforming for crowdsourced bistatic satellite isac with 11m. *IEEE Journal on Selected Areas in Communications*, 44:2348–2364, 2026. 2
- [25] Oscar Mañas, Alexandre Lacoste, Xavier Giró-i Nieto, David Vazquez, and Pau Rodríguez. Seasonal contrast: Un-supervised pre-training from uncurated remote sensing data. In *Proceedings of the IEEE/CVF International Conference on Computer Vision (ICCV)*, pages 9414–9423, 2021. 6
- [26] Gengchen Mai, Yiqun Xie, Xiaowei Jia, Ni Lao, Jinneng Rao, Qing Zhu, Zeping Liu, Yao-Yi Chiang, and Junfeng Jiao. Towards the next generation of geospatial artificial intelligence. *International Journal of Applied Earth Observation and Geoinformation*, 136:104368, 2025. 1, 3
- [27] Clive Tinashe Marimo, Benedikt Blumenstiel, Maximilian Nitsche, Johannes Jakubik, and Thomas Brunschweiler. Beyond the visible: Multispectral vision-language learning for earth observation. In *ECML PKDD*, 2025. 2, 3, 6, 7, 8
- [28] Valerio Marsocci, Yuru Jia, Georges Le Bellier, David Kerekes, Liang Zeng, Sebastian Hafner, Sebastian Gerard, Eric Brune, Ritu Yadav, Ali Shibli, Heng Fang, Yifang Ban, Maarten Vergauwen, Nicolas Audebert, and Andrea Nascetti. Pangaea: A global and inclusive benchmark for geospatial foundation models, 2025. 6
- [29] Iulia Coca Neagoe, Daniela Faur, Corina Vaduva, and Mihai Datcu. Band reconstruction using a modified unet for sentinel-2 images. *IEEE Journal of Selected Topics in Applied Earth Observations and Remote Sensing*, 16:6739–6757, 2023. 2
- [30] Mubashir Noman, Muzammal Naseer, Hisham Cholakkal, Rao Muhammad Anwar, Salman Khan, and Fahad Shahbaz Khan. Rethinking Transformers Pre-training for Multi-Spectral Satellite Imagery. In *2024 IEEE/CVF Conference on Computer Vision and Pattern Recognition (CVPR)*, pages 27811–27819, Los Alamitos, CA, USA, 2024. IEEE Computer Society. 3
- [31] Maxime Oquab, Timothée Darcet, Theo Moutakanni, Huy V. Vo, Marc Szafraniec, Vasil Khalidov, Pierre Fernandez, Daniel Haziza, Francisco Massa, Alaaeldin El-Nouby, Russell Howes, Po-Yao Huang, Hu Xu, Vasu Sharma, Shang-Wen Li, Wojciech Galuba, Mike Rabbat, Mido Assran, Nicolas Ballas, Gabriel Synnaeve, Ishan Misra, Herve Jegou, Julien Mairal, Patrick Labatut, Armand Joulin, and Piotr Bojanowski. Dinov2: Learning robust visual features without supervision, 2023. 3
- [32] Alec Radford, Jong Wook Kim, Chris Hallacy, Aditya Ramesh, Gabriel Goh, Sandhini Agarwal, Girish Sastry, Amanda Askell, Pamela Mishkin, Jack Clark, Gretchen Krueger, and Ilya Sutskever. Learning transferable visual models from natural language supervision. In *Proceedings of the 38th International Conference on Machine Learning*, pages 8748–8763. PMLR, 2021. 5, 7, 8
- [33] Colorado J Reed, Ritwik Gupta, Shufan Li, Sarah Brockman, Christopher Funk, Brian Clipp, Kurt Keutzer, Salvatore Candido, Matt Uyttendaele, and Trevor Darrell. Scale-MAE: A Scale-Aware Masked Autoencoder for Multiscale Geospatial Representation Learning. In *2023 IEEE/CVF International Conference on Computer Vision (ICCV)*, pages 4065–4076, Los Alamitos, CA, USA, 2023. IEEE Computer Society. 3
- [34] Rajagopalan Rengarajan, Michael Choate, Md Nahid Hasan, and Alex Denevan. Co-registration accuracy between landsat-8 and sentinel-2 orthorectified products. *Remote Sensing of Environment*, 301:113947, 2024. 2
- [35] Oriane Siméoni, Huy V. Vo, Maximilian Seitzer, Federico Baldassarre, Maxime Oquab, Cijo Jose, Vasil Khalidov, Marc Szafraniec, Seungeun Yi, Michaël Ramamonjisoa, Francisco Massa, Daniel Haziza, Luca Wehrstedt, Jianyuan Wang, Timothée Darcet, Théo Moutakanni, Leonel Sentana, Claire Roberts, Andrea Vedaldi, Jamie Tolan, John Brandt, Camille Couprie, Julien Mairal, Hervé Jégou, Patrick Labatut, and Piotr Bojanowski. DINOv3, 2025. 5, 6, 7, 8
- [36] Oscar SKEAN, Md Rifat Arefin, Dan Zhao, Niket Nikul Patel, Jalal Naghiyev, Yann LeCun, and Ravid Shwartz-Ziv. Layer by layer: Uncovering hidden representations in language models. In *Forty-second International Conference on Machine Learning*, 2025. 2, 5
- [37] Sagar Soni, Akshay Dudhane, Hiyam Debary, Mustansar Fiaz, Muhammad Akhtar Munir, Muhammad Sohail Danish, Paolo Fraccaro, Campbell D Watson, Levente J Klein, Fahad Shahbaz Khan, and Salman Khan. Earthdial: Turning multi-sensory earth observations to interactive dialogues. In *Proceedings of the IEEE/CVF Conference on Computer Vision and Pattern Recognition (CVPR)*, pages 14303–14313, 2025. 1, 6, 7
- [38] Gencer Sumbul, Marcela Charfuelan, Begüm Demir, and Volker Markl. Bigearthnet: A large-scale benchmark archive for remote sensing image understanding. In *IGARSS 2019 - 2019 IEEE International Geoscience and Remote Sensing Symposium*, pages 5901–5904, 2019. 1, 6
- [39] Xian Sun, Peijin Wang, Wanxuan Lu, Zicong Zhu, Xiaonan Lu, Qibin He, Junxi Li, Xuee Rong, Zhujun Yang, Hao

- Chang, Qinglin He, Guang Yang, Ruiping Wang, Jiwen Lu, and Kun Fu. Ringmo: A remote sensing foundation model with masked image modeling. *IEEE Transactions on Geoscience and Remote Sensing*, 61:1–22, 2023. 3
- [40] Michael Tschannen, Alexey Gritsenko, Xiao Wang, Muhammad Ferjad Naeem, Ibrahim Alabdulmohsin, Nikhil Parthasarathy, Talfan Evans, Lucas Beyer, Ye Xia, Basil Mustafa, Olivier Hénaff, Jeremiah Harmsen, Andreas Steiner, and Xiaohua Zhai. Siglip 2: Multilingual vision-language encoders with improved semantic understanding, localization, and dense features, 2025. 1, 3
- [41] Yi Wang, Nassim Ait Ali Braham, Zhitong Xiong, Chenying Liu, Conrad M. Albrecht, and Xiao Xiang Zhu. Ssl4eos12: A large-scale multimodal, multitemporal dataset for self-supervised learning in earth observation [software and data sets]. *IEEE Geoscience and Remote Sensing Magazine*, 11(3):98–106, 2023. 1
- [42] Zhecheng Wang, Rajanie Prabha, Tianyuan Huang, Jiajun Wu, and Ram Rajagopal. Skyscript: a large and semantically diverse vision-language dataset for remote sensing. In *Proceedings of the Thirty-Eighth AAAI Conference on Artificial Intelligence and Thirty-Sixth Conference on Innovative Applications of Artificial Intelligence and Fourteenth Symposium on Educational Advances in Artificial Intelligence*. AAAI Press, 2024. 3, 7, 8
- [43] Xingxing Weng, Chao Pang, and Gui-Song Xia. Vision-language modeling meets remote sensing: Models, datasets, and perspectives. *IEEE Geoscience and Remote Sensing Magazine*, 13(3):276–323, 2025. 3
- [44] Zhitong Xiong, Yi Wang, Fahong Zhang, Adam J Stewart, Joëlle Hanna, Damian Borth, Ioannis Papoutsis, Bertrand Le Saux, Gustau Camps-Valls, and Xiao Xiang Zhu. Neural plasticity-inspired foundation model for observing the Earth crossing modalities. *arXiv preprint arXiv:2403.15356*, 2024. 3
- [45] Zhitong Xiong, Fahong Zhang, Yi Wang, Yilei Shi, and Xiao Xiang Zhu. Earthnets: Empowering artificial intelligence for earth observation. *IEEE Geoscience and Remote Sensing Magazine*, pages 2–36, 2024. 1
- [46] Zhitong Xiong, Yi Wang, Weikang Yu, Adam J Stewart, Jie Zhao, Nils Lehmann, Thomas Dujardin, Zhenghang Yuan, Pedram Ghamisi, and Xiao Xiang Zhu. Dofa-clip: Multimodal vision-language foundation models for earth observation, 2025. 1, 2, 3, 6, 7, 8
- [47] Z. Yuan, Z. Xiong, L. Mou, and X. X. Zhu. Chatearthnet: a global-scale image–text dataset empowering vision–language geo-foundation models. *Earth System Science Data*, 17(3):1245–1263, 2025. 1
- [48] Xiaohua Zhai, Xiao Wang, Basil Mustafa, Andreas Steiner, Daniel Keysers, Alexander Kolesnikov, and Lucas Beyer. Lit: Zero-shot transfer with locked-image text tuning. In *2022 IEEE/CVF Conference on Computer Vision and Pattern Recognition (CVPR)*, pages 18102–18112, 2022. 2, 5
- [49] Jingyi Zhang, Jiaying Huang, Sheng Jin, and Shijian Lu. Vision-language models for vision tasks: A survey. *IEEE Transactions on Pattern Analysis and Machine Intelligence*, 46(8):5625–5644, 2024. 1
- [50] Zilun Zhang, Tiancheng Zhao, Yulong Guo, and Jianwei Yin. Rs5m and georsclip: A large-scale vision- language dataset and a large vision-language model for remote sensing. *IEEE Transactions on Geoscience and Remote Sensing*, 62:1–23, 2024. 2, 3, 6, 7, 8

Spectrally Distilled Representations Aligned with Instruction-Augmented LLMs for Satellite Imagery

Supplementary Material

The Supplementary Material is organized as follows. Sec. 7 discusses limitations and future work; Sec. 8 reports additional quantitative results on downstream tasks; Sec. 9 provides further qualitative examples; Sec. 10 describes the baselines and downstream datasets; and Sec. 11 details the implementation to facilitate reproducibility.

7. Limitations and Future Work

This work is constrained by two limitations: reliance on optical (RGB) imagery and the cost of text encoding at inference. Our method studies image-text alignment in optical remote sensing and assumes RGB-only inputs at test time. Therefore, sensors such as SAR or thermal are not considered, which can limit robustness under cloud cover, haze, or night conditions. We chose this setting because RGB is the most commonly available modality. A promising extension is to incorporate additional sensors into the teacher-alignment framework so that the RGB pathway inherits cross-modal priors. On the efficiency side, using LLMs as the text encoder increases latency and memory during inference. However, in typical deployments this cost is largely amortized by pre-computing and caching text embeddings for the label vocabulary and prompt sets. In addition, the method is compatible with model compression techniques such as quantization, which can reduce runtime and memory footprint while preserving the accuracy.

8. Additional Quantitative Results

We report F1 scores for zero-shot classification and for the linear-probe setting.

In Tab. 5, we compare zero-shot classification F1 across three satellite benchmarks, namely EuroSAT, BigEarthNet, and ForestNet, grouped by training paradigm (generative vs. contrastive) and input modality (RGB vs. MS). Generative models underperform the best contrastive approaches on all datasets. Among contrastive baselines, remote sensing-aware methods such as GeoRSCLIP, SkyCLIP, and DOFA-CLIP reduce the gap to general-purpose vision-language models, and multi-spectral inputs help in some cases, for example DOFA-CLIP with multi-spectral input on ForestNet. Despite using only RGB inputs, SATtxt with RGB input attains the best results on all three datasets, reaching 73.40 on EuroSAT, 60.18 on BigEarthNet, and 19.89 on ForestNet, and surpassing both RGB and multi-spectral competitors. These results highlight the effectiveness of spectral-aware pre-training even without MS inputs.

Table 5. Zero-shot classification (F1 \uparrow) on three satellite benchmarks. “-” denotes an unsupported task or an inapplicable dataset.

Training Approach	Model	Input	Zero-shot Classification		
			EuroSAT	BigEarthNet	ForestNet
Generative	GeoChat	RGB	30.82	14.62	6.15
	EarthDial	MS	57.26	31.80	8.11
Contrastive	CLIP	RGB	40.35	54.85	8.30
	RemoteCLIP	RGB	27.34	52.28	8.50
	GeoRSCLIP	RGB	47.04	58.80	8.27
	SkyCLIP	RGB	48.50	52.88	9.73
	DINOv3txt	RGB	46.29	57.30	14.29
	FT-DINOv3txt	RGB	53.26	58.14	15.37
	DOFA-CLIP	RGB	63.73	58.96	12.33
	DOFA-CLIP	MS	42.18	56.58	15.35
	Llama3-MS-CLIP	MS	64.27	59.63	-
	SATtxt (ours)	RGB	73.40	60.18	19.89

Table 6. Linear-probe (F1 \uparrow) on EuroSAT, BigEarthNet (10% and 100%), and ForestNet. “-” denotes an inapplicable dataset.

Training Approach	Model	Input	EuroSAT	BigEarthNet		ForestNet
				10%	100%	
MIM	SpectralGPT	MS	95.96	60.70	69.93	-
	Terramind	MS	91.65	65.49	74.08	37.30
Contrastive	CLIP	RGB	91.83	45.32	64.12	24.02
	RemoteCLIP	RGB	95.02	45.40	64.24	18.35
	GeoRSCLIP	RGB	95.76	60.71	70.65	34.74
	SkyCLIP	RGB	93.13	58.21	44.15	16.09
	DINOv3txt	RGB	94.76	26.86	45.28	41.49
	FT-DINOv3txt	RGB	95.46	58.31	48.64	41.13
	DOFA-CLIP	RGB	96.88	59.35	65.59	12.17
	DOFA-CLIP	MS	94.50	66.21	69.41	13.35
	Llama3-MS-CLIP	MS	94.85	68.15	68.04	-
	SATtxt (ours)	RGB	97.99	70.43	74.49	45.98

Tab. 6 presents linear-probe F1 on EuroSAT, BigEarthNet with 10% and full supervision, and ForestNet. The comparison includes masked-image-modeling pre-training, represented by SpectralGPT and Terramind, together with contrastive baselines. MIM approaches are competitive, particularly on EuroSAT and BigEarthNet, yet several contrastive models show substantial gains when increasing label fractions. SATtxt with RGB input achieves the best performance in every setting, namely 97.99 on EuroSAT, 70.43 and 74.49 on BigEarthNet with 10% and 100% labels, and 45.98 on ForestNet, outperforming the strongest multi-spectral and RGB baselines including DOFA-CLIP and Llama3-MS-CLIP. Gains in both low-label and full-label regimes indicate that SATtxt learns features that are label efficient and linearly separable, and the strong ForestNet result demonstrates robustness real-world forest categories. Overall, the linear-probe trends align with the zero-

shot findings, showing that spectral-aware contrastive pre-training yields consistently strong and robust representations across multiple optical satellite datasets.

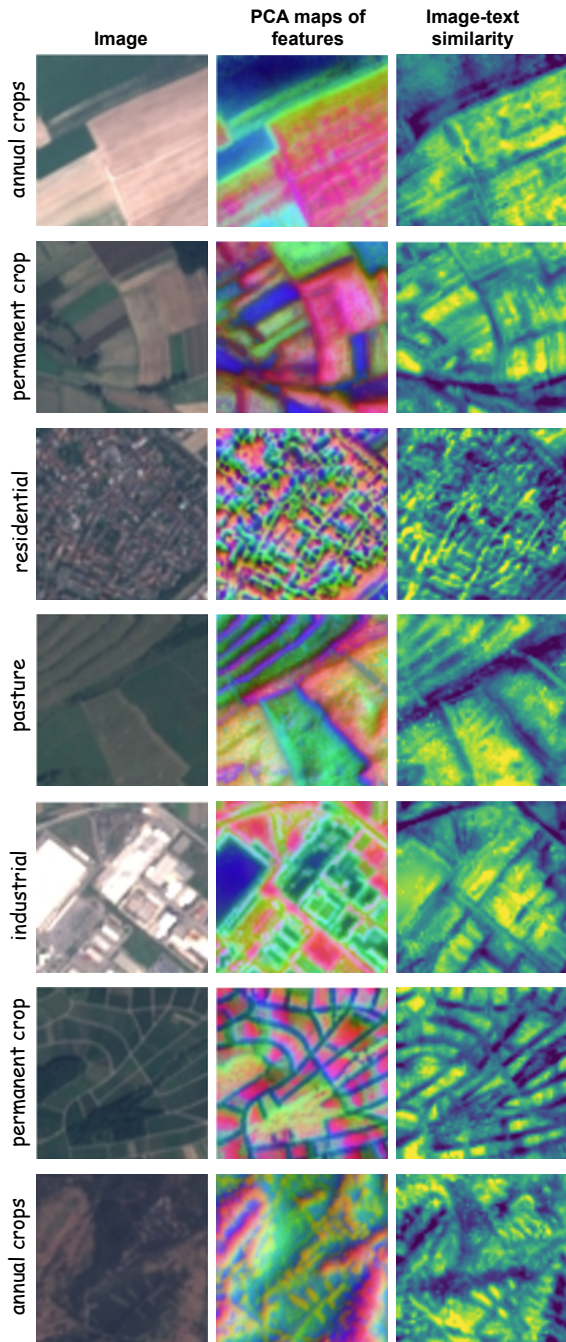


Figure 8. PCA-based feature map visualizations and patch-wise image-text similarity maps with labels.

9. Additional Qualitative Results

We visualize the model’s feature maps following the DINOv3 protocol. Using a patch size of 16, we first resize each image to 1024×1024 pixels, resulting in feature maps of spatial resolution 64×64 at the last layer. We then perform principal component analysis (PCA) on these feature maps and project them onto the first three principal components to obtain pseudo-RGB visualizations, which are bilinearly upsampled back to the original image resolution. In addition, we visualize patch-wise image-text similarity with labels. As shown in Fig. 8, the SATtxt produces well-structured PCA feature maps and object-focused image-text similarity maps.

10. Baseline & Dataset Details

Baseline. Tab. 7 summarizes the baseline models evaluated in this study. We include both general-purpose vision-language models and those specifically adapted for remote sensing imagery. All models are configured using their publicly available checkpoints that provide the best performance.

Table 7. Model configurations used in our experiments.

Model	Backbone
CLIP	ViT-L-14
RemoteCLIP	ViT-L-14
GeoRSCLIP	ViT-B-32
SkyCLIP	ViT-L-14
Llama3-MS-CLIP	ViT-B-16
DOFA-CLIP	ViT-L-14
DINOv3txt	ViT-L-16
SATtxt (ours)	ViT-L-16

Dataset. Tab. 8 summarizes the downstream datasets evaluated in this study. We consider four publicly available benchmarks spanning two optical satellite sensors: Sentinel-2 and Landsat-8. For each dataset, we report the number of training/validation/test samples, spectral bands, and classes. Note that BigEarthNet-10% and BigEarthNet-100% share the same test split. EuroSAT includes 13 spectral bands, whereas BigEarthNet includes 12 bands. For multi-spectral inputs on EuroSAT and BigEarthNet, following Clive *et al.* [27], we exclude bands with mismatched spatial resolutions or redundant information [7] and use the 10-band subset {B02 - B08, B8A, B11, B12} to ensure fair and consistent comparisons across multi-spectral models. To assess cross-sensor generalization, we additionally evaluate on ForestNet [15], collected with Landsat-8, which provides 5 spectral bands and 12 classes in a single-label setting.

Table 8. Downstream datasets used in this study.

Details	EuroSAT	BigEarthNet-10%	BigEarthNet-100%	ForestNet
# Training Samples	16,200	25,000	269,695	6,464
# Validation Samples	5,400	10,000	123,723	989
# Test Samples	5,400	125,866	125,866	993
# Spectral Bands	13	12	12	5
# Classes	10	19	19	12

11. Additional Implementation Details

Pre-training Implementation. In the first Stage (SRD), the multi-spectral (MS) teacher (*i.e.*, SpectralGPT) operates at the fixed 128×128 resolution imposed by its pre-trained checkpoint. Accordingly, we set the teacher’s global resolution to 128×128 with two views. Following DI-NOv3, the student receives eight local views at 96×96 . We use softmax temperatures of 0.1 for the student and 0.06 for the teacher, with a center momentum of 0.9. For data augmentation, we employ multi-crop augmentation that samples two shared random-resized global crops for RGB and MS plus eight RGB-only local crops, applying view-dependent color jitter, grayscale, blur and solarization to RGB while leaving MS geometrically aligned but photometrically clean, followed by per-modality normalization. Training proceeds for 5 epochs with a batch size of 128 using AdamW, an initial learning rate of 5×10^{-4} , and cosine decay. In the second stage (SGI-LLM), we employ the simple instruction set summarized in Tab. 9. Training runs for 10 epochs with a batch size of 1024 under AdamW optimizer, with an initial learning rate of 4×10^{-5} and cosine decay. Complete configuration details for Stage 1 (SRD) and Stage 2 (SGI-LLM) are provided in Fig. 9 and Fig. 10, respectively.

Linear-probe Implementation. Unlike zero-shot evaluation, linear-probe results can vary across models because of differences in training hyperparameters and preprocessing. To ensure comparability, we adopt the PANGAEA configuration with minimal preprocessing: resizing, selecting the RGB channels for models that accept RGB inputs, and standard mean-std normalization. All linear probes are trained for 30 epochs with a batch size of 128 using AdamW (learning rate 1×10^{-4} , $\beta = (0.9, 0.999)$, weight decay 0.05) and a multi-step learning-rate scheduler.

```

1 net:
2   _target_: models.SRD_module.SRD
3   student_encoder_backbone: facebook/dinov3-vitl16-pretrain-sat493m.pth
4   teacher_encoder_backbone: danfenghong/IEEE_TPAMI_SpectralGPT/SpectralGPT+.pth
5   student_projector: transformer
6   student_projector_nlayers: 2
7   embed_dim: 1024
8   lock_student: true
9   lock_teacher: true
10
11 criterion:
12   _target_: losses.SRDLoss
13   feature_dim: 1024
14   prototypes_dim: 8192
15   T_teacher: 0.06 # teacher temperature
16   T_student: 0.10 # student temperature
17   center_momentum: 0.9 # EMA momentum for logit center
18   eps: 1e-6
19
20 data:
21   _target_: data.ssl4eos12.Ssl4eos12
22   batch_size: 128
23   modalities: [S2RGB, S2L2A]
24   S2RGB_means: [0.48145466, 0.4578275, 0.40821073]
25   S2RGB_stds: [0.26862954, 0.26130258, 0.27577711]
26   S2L2A_means: [1924.863, 2184.553, 2340.936, 2671.402,
27                3240.082, 3468.412, 3563.244, 3627.704, 3416.714, 2849.625]
28   S2L2A_stds: [1201.092, 1219.943, 1397.225, 1400.035,
29                1373.136, 1429.17, 1485.025, 1447.836, 1471.002, 1365.307]
30   global_size: 128
31   n_globals: 2 # number of global views
32   local_size: 96
33   n_locals: 8 # number of local views
34
35 optimizer:
36   _target_: torch.optim.AdamW
37   lr: 5e-4
38   weight_decay: 0.01
39   betas: [0.9, 0.999]
40   eps: 1e-8
41
42 scheduler:
43   _target_: schedulers.WarmupCosineWithGroupMultipliers
44   warmup_epochs: 1
45   max_epochs: 5
46   warmup_start_lr: 1e-6
47   eta_min: 1e-6

```

Figure 9. Stage 1 (SRD) configuration details.

- “Represent this satellite caption to align with its image”
- “Represent this overhead description for image-text retrieval”
- “Remote sensing caption to match its satellite image”
- “Overhead scene description for image-text alignment”
- “Produce a caption representation suitable for visual search over satellite images”

Table 9. The list of instructions for vision-language alignment.

```

1 net:
2   _target_: models.SATtxt_module.SATtxt_Module
3   embed_dim: 2048           # vision embedding dimension
4   text_hidden: 4096        # text embedding dimension
5   image_backbone: facebook/dinov3-vitl16-pretrain-sat493m.pth
6   vision_projector: SRD_pretrained_projector.pt
7   text_backbone: McGill-NLP/LLM2Vec-Meta-Llama-3-8B-Instruct-mntp
8   text_proj_type: linear
9   lock_vision: true        # freeze image backbone
10  lock_text: true          # freeze text backbone
11
12 criterion:
13   _target_: losses.InfoNCELoss
14   initial_temperature: 0.07
15   learnable_temperature: true
16   symmetric_loss: true
17
18 data:
19   _target_: data.ssl4eos12.Ssl4eos12
20   modalities: [S2RGB, precomputed_text_embeddings]
21   batch_size: 1024
22   channels: 3
23   image_size: 224
24   S2RGB_means: [0.48145466, 0.4578275, 0.40821073]
25   S2RGB_stds: [0.26862954, 0.26130258, 0.27577711]
26
27 optimizer:
28   _target_: torch.optim.AdamW
29   lr: 4e-5
30   weight_decay: 0.01
31   betas: [0.9, 0.999]
32   eps: 1e-8
33
34 scheduler:
35   _target_: schedulers.LinearWarmupCosineAnnealingLR
36   warmup_epochs: 2
37   max_epochs: 10
38   warmup_start_lr: 1e-5
39   eta_min: 1e-6

```

Figure 10. Stage 2 (SGI-LLM) configuration details.